2019-05-01

Effect of viscoelasticity on interfacial stress transfer mechanism in biocomposites: A theoretical study of viscoelastic shear lag model

Li, Long-yuan

10.1016/j.compositesb.2018.11.086
Composites Part B: Engineering
Elsevier

Composites Part B: Engineering 164, 297-308,
doi:https://doi.org/10.1016/j.compositesb.2018.11.086.
Received 3 June 2018; Received in revised form 2 November 2018; Accepted 20 November 2018

Effect of viscoelasticity on interfacial stress transfer mechanism in biocomposites: A theoretical study of viscoelastic shear lag model

Jiayu Wu[a,b], Hong Yuan[a,*], Long-yuan Li[b]

[a]MOE Key Laboratory of Disaster Forecast and Control in Engineering, Institute of Applied Mechanics, Jinan University, Guangzhou 510632, China

[b]School of Engineering, University of Plymouth, Drake Circus, Plymouth PL4 8AA, UK

*Corresponding author, E-mail addresses: tyuanhong@jnu.edu.cn

Abstract: Biocomposites with regularly staggered alignment microstructure are frequently observed in natural biological tissues, and exhibit superior mechanical behavior. Owing to their viscoelastic nature, biocomposites exhibit stress rate-dependent stiffness function and mechanical behavior. In this paper, a linear viscoelastic shear lag model (SLM) is proposed to illustrate the micromechanical behavior of biocomposites under triangular loading pulse. Theoretical and numerical results are derived to predict the deformation and stress transfer between fibers and interfibrous matrix while the biocomposites are transiently stretched. The results from the analytical and numerical solutions demonstrate that how the fiber overlap length and loading rate affect the stress transfer and mechanical properties of biocomposties. The structure-property correlation is illustrated for viscoelastic biomaterials under transient loading, and the existence of characteristic length of soft matter with viscoelastic property is involved in load transfer mechanism between the adjacent reinforcements in transient regime, which optimizes the load transfer mechanism between the adjacent reinforcements. Furthermore, we found that discontinuous fibril model could ensure large relative sliding deformation, helping dissipate energy, protecting fibril from overall damage, and achieving high ductility and high toughness, which can provide beneficial design strategies for engineering fiber reinforced composites.

Keywords: Biocomposites; Shear lag model; Mechanics of composite interface; Viscoelastic model; Mechanical response.

1. Introduction

1.1. Research objective

Synthetic engineering materials with exceptional strength and toughness are a crucial requirement for many engineering structures; yet these mechanical properties are normally mutually exclusive [1]. The quest for addressing the conflict between high strength and high toughness has been prompting scientists to resort to

natural materials. Over millions of years of evolution by natural selection, unidirectional biocomposites with regularly staggered alignment microstructure are frequently observed in natural biological tissues (see Fig. 1) [2, 3], such as bone [4, 5], nacre [1], tendon [6] and axon [7], etc. Biocomposites have been found to exhibit an excellent mechanical balance with high strength and high toughness simultaneously [4, 8, 9]. In such microstructures, the stiff fiber, with relatively low fracture toughness and low strength-to-modulus ratio, is responsible for carrying a majority of the tensile stress. On the other hand, the compliant crosslinks of matrix, with relatively high ductility and high strength-to-modulus ratio, are inclined to take the comparatively greater part of the shear strain [3, 10, 11].

The purpose of this paper is to theoretically and numerically explore and address the questions with regards to viscoelastic biocomposites owing to regular staggered alignment microstructure considering that the most elementary level of architecture is under transient loading. (1) Does there exist a structure-property correlation for the viscoelastic biomaterials under transient loading? (2) The characteristic length of bone and nacre exists under quasi-static loading conditions, which optimizes stiffness and strength; is there any associated characteristic length of soft matter with viscoelastic property involved in the mechanism of stress transmission between the neighboring reinforcements in transient regime? (3) As had been proposed by Gao et al. [2], building blocks in hard tissues are at nanoscales under quasi-static loading conditions; is the identical argument available for soft tissues under transient loading? With the aim of answering these questions, the following methods for analysis need to be applied: (a) establishing linear viscoelastic SLM for staggered alignment microstructural biomaterials under impact loading considering linear viscoelastic behavior, (b) identification of the characteristic length involved in these cases, (c) predicting characteristic length for collagen fibrils in tendon having staggered alignment microstructure as its fibril level, (d) providing new insights into the effect of applied stress rate on viscoelastic biocomposites.

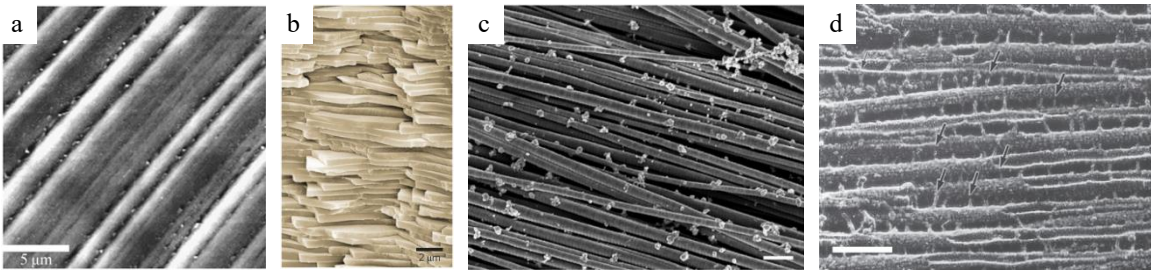

Fig. 1 Various geometries of fibrous structure in biological systems. (a) Bone collagen fibers [5]; (b) Nacre composed of aragonite platelets surrounded by thin layers of organic materials composed of proteins [4]; (c) Collagen fibrils with regular parallel arrays in tendon (Scale bar of 500 nm) [6]. (d) Electron micrograph of axonal microtubules connected by tau protein (Scale bar of 100 nm) [7].

1.2. Literature review

The well-known “brick-and-mortar” architecture, with discontinuous staggered stiff platelet embedded in a soft protein matrix, can be introduced to shed light on the load transfer mechanism of biocomposites. In order to characterize the mechanical interaction behavior of the platelets, Gao et al. [2, 12] proposed a tension–shear chain (TSC) model to explicitly elucidate the path of load transfer in the biocomposites,

where the fiber carry tensile load and the matrix transfers load between fibers via shear. Furthermore, TSC model established the relationship between the stiffness, aspect ratio of minerals, mineral volume fraction and material properties. It is noteworthy that many researchers utilized SLM to predict load transmission in the fiber reinforced composite under static or quasi-static loading conditions.

The SLM was originally proposed by Cox [13], which is commonly applied to represent fiber reinforced composite material consisting of discontinuous fibers embedded in a softer matrix as a powerful analytical method for elucidating stress transfer and crack propagation between fibers and matrix [14]. The model has been widely used in various fields, such as materials science [8, 15, 16], geology [17, 18], structural engineering [19, 20] and biomechanics [21-23]. There are broad prospects for development.

Interfacial shear stress distribution is a key parameter to determine the efficiency of load transfer from the polymer matrix to the fibers. Recently, researchers focused more on the constitutive relation of the matrix, resulting in various bond-slip models being accurately employed to improve the interfacial shear stress between the fibers and matrix (see Fig. 2). Chen et al. [24] discussed the characteristic length for efficient stress transfer in staggered biocomposites via the derivation of an elastic model (Fig. 2a) followed by numerical simulations. Wei et al. [8] proposed a criterion by using elasto-plastic model (Fig. 2d), which reveals the existence of a unique overlap length in biocomposites that contributes to an optimization on both strength and toughness fronts. Elastic-linear softening model (Fig. 2e) without the effect of friction after debonding is a popular bond-slip model [14, 25-28], which is usually applied by many researchers. However, some researchers [27, 29] considered the interfacial friction behavior between fiber and matrix, and postulated an elastic-linear softening-frictional model (Fig. 2f). In a similar manner, elastic-frictional model (Fig. 2g) was employed by Sanborn and Prévost [29] to investigate the platelet pullout process. For the sake of better understanding of the debonding process of fiber-matrix interface, Nian et al. [30] developed a bilinear traction separation and the Coulomb friction model (Fig. 2h) to capture different levels of plasticity at the interface. Moreover, elastic-hardening-softening model (Fig. 2i) was also proposed [31, 32]. Investigations using shear lag model with piecewise linear model (Fig. 2j) and multilinear model (Fig. 2k) were carried out by Pimenta and Robinson [33], Zhandarov and Mäder [34], respectively. In addition, nonlinear cohesive law (Fig. 2l) was applied for the single carbon nanotube pullout model [35]. Obviously, researchers attempt to find out the accurate interfacial constitutive relations for different adhesive materials. It should be noted that extensive literature exists on quantifying the role of microstructure and material parameters on the behavior of staggered architecture; however, most of the work was only under static or quasi-static loading conditions. There are very limited studies that address the factors responsible for this behavior under transient rates of loading. Dutta et al. [15, 36] constructed the mechanical dynamic model, and gave the impressive analytical results.

Notably, these elastic and elasto-plastic constitutive models, as depicted in Fig. 2, lead to structure deformation instantaneously. Assuming that these interfacial constitutive relations are employed to elucidate the load transmission and crack propagation in biological composite materials, some limitations still exist, as they could not reflect the mechanical behavior of creep and stress relaxation. Nevertheless, soft material of biological tissue is sensitive to loading rate. Thus, physical property of viscosity needs to be considered in the analytical model of natural biological materials. The modified shear lag models have been recently developed for the application of tissues biomechanics. As for hard tissues, with high stiffness

and low viscosity, loading rate has little influence on the mechanical behavior of hard tissues. Soft tissues, with low stiff and high viscosity, are sensitive to loading rate. Furthermore, soft tissues exhibit stress rate-dependent breaking and stiffness function. Ahmadzadeh et al. [21] utilized bilinear elastic model (Fig. 2b) to modify shear lag model for tendon. By using elastic model (Fig. 2a), rigid plastic model (Fig. 2c), elasto-plastic model (Fig. 2d), Szczesny and Elliott [22, 23] applied shear lag model to elucidate the fundamental mechanisms of deformation and stress transfer for tendon. Obviously, elasto-plastic constitutive models are insufficient to describe the mechanical behavior of biocomposites.

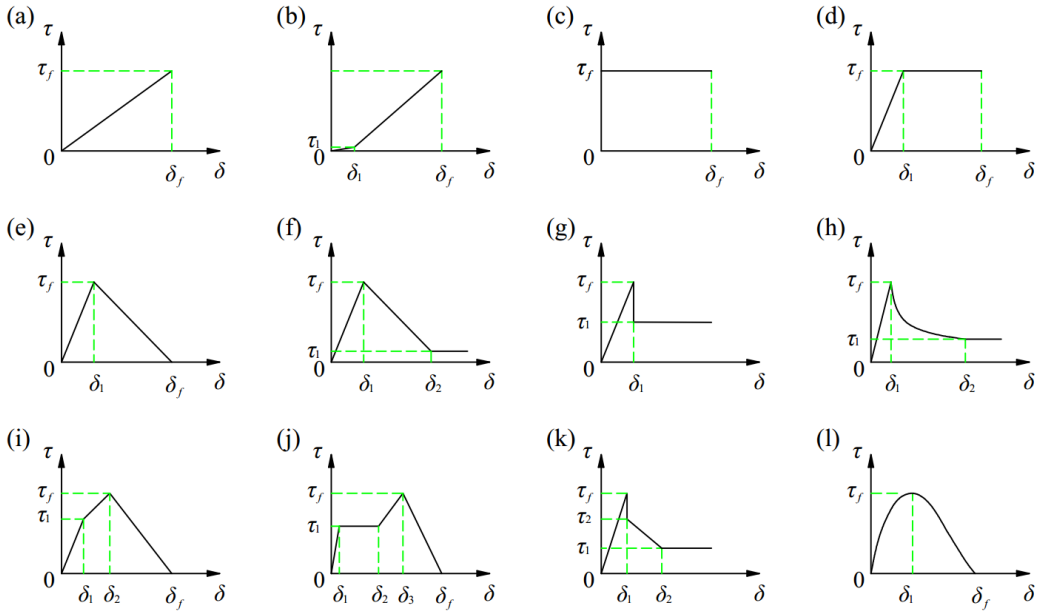

Fig. 2 Common constitutive models for fiber-matrix interface. (a) Elastic-brittle model; (b) Bilinear elastic model; (c) Rigid plastic model; (d) Elasto-plastic model; (e) Elastic-linear softening model; (f) Elastic-linear softening-frictional model; (g) Elastic- frictional model; (h) Bilinear traction separation and the Coulomb friction model; (i) Elastic-hardening-softening model; (j) Piecewise linear model; (k) Multilinear model; (l) Nonlinear model.

2. Fundamental Formulas

2.1. General features

To characterize the deformation and stress transmission mechanisms mainly caused from impact loading, creep and stress relaxation in fibrous biological structures, three common types of linear viscoelastic SLM are normally established to analyze the mechanical behavior between biological fibers and interfibrous matrix. Before theoretical derivations, the following assumptions should be taken into consideration:

(i) The shear modulus of interfibrous matrix is several orders of magnitude smaller than the elastic modulus of fiber such that the interfibrous matrix could not transfer any normal stress between the adjacent fibers; the stress in the longitudinal direction can only be transferred via shear in interfibrous matrix.

(ii) The stiffest discontinuous fibers are surrounded by interstitial fluid, or weakest-linked by protein,

proteoglycans or glycosaminoglycans, etc., generating large deformation and large deformation rate in the interfibrous matrix; and the stiff fibers are linear elastic.

(iii) Under tensile force, the deformation of biocomposites is mainly in longitudinal dimension.

(iv) The adjacent fibers are parallel arranged along the longitudinal direction, and overlap about half of their total length regularly.

(v) The mass of the fibril is extremely small so that it can be neglected in the mechanical modeling.

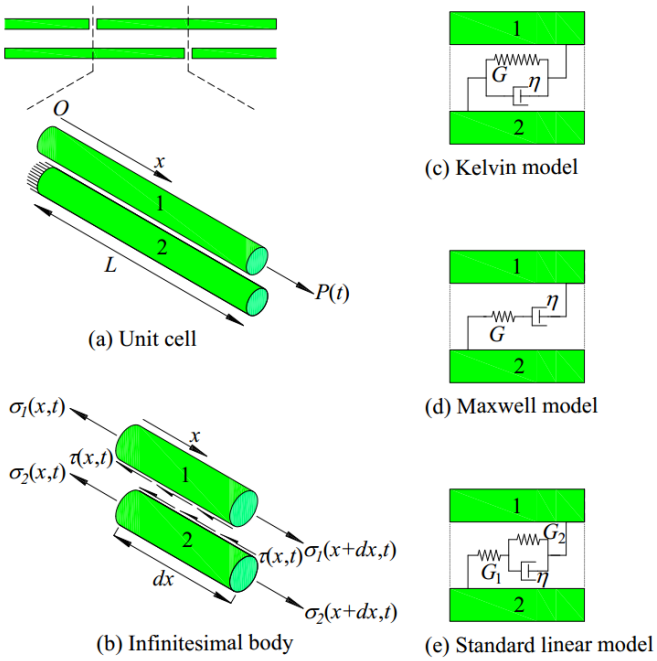

Fig. 3 (a) A unit cell with two adjacent fibers used in the shear lag model; (b) Equilibrium in infinitesimal body; (c) A Kelvin viscoelastic model composed of a spring and a dashpot in parallel considered for interfibrous matrix; (d) A Maxwell model containing a spring and dashpot in series; (e) A standard linear viscoelastic model containing a spring in series with a Kelvin unit.

Table 1 Symbols used in the viscoelastic shear lag model

Variable	Brief description
E_f	Fiber Young's modulus
G	Interfibrous matrix shear modulus
η	Interfibrous matrix viscosity coefficient
L	Half-length of fiber
L_C	Characteristic load transfer length
r	Fiber radius
h	Distance between adjacent fibers surfaces
δ	Relative displacement between adjacent fibers
u_i	Displacement of i-th fiber
ε_i	Normal strain of i-th fiber
σ_i	Normal stress of i-th fiber
τ	Interfibrous matrix shear stress

γ	Interfibrous matrix shear strain
P	Force at the midpoint of fiber
c_f	Fibrous volume fraction

When a biocomposite is under tensile loading, stress is transferred from one fiber to the adjacent fibers through interfibrous matrix, which is subjected to shear stress and leads to relative sliding between fibers. Let δ be the relative sliding between adjacent fibers, which can be expressed as

$$\delta(x,t) = u_1(x,t) - u_2(x,t) \tag{1}$$

where $u_1(x,t)$ and $u_2(x,t)$ are the displacement of the 1st and 2nd fibers, respectively.

The parameters used in this viscoelastic shear lag model are list in Table 1. A Cartesian coordinate system is placed at the midpoint of a fiber, in such a way that the length direction of fibers is along x-direction, as depicted in Fig. 3b. Interfibrous matrix shear strain γ can be expressed as follows

$$\gamma = \frac{u_1(x,t) - u_2(x,t)}{h} = \frac{\delta(x,t)}{h} \tag{2}$$

where h is the surface-to-surface distance between the adjacent fibers.

The unit cell (Fig. 3a) and infinitesimal body (Fig. 3b) show the two adjacent fibers, in which each fiber is affected by its adjacent fibers. A shear stress $\tau(x,t)$ acts over the entire fiber circumference, resulting in the equilibrium equations as follows [22]

$$\frac{\partial \sigma_1(x,t)}{\partial x} = \frac{2\tau(x,t)}{r} \tag{3}$$

$$-\frac{\partial \sigma_2(x,t)}{\partial x} = \frac{2\tau(x,t)}{r} \tag{4}$$

where r is the radius of the fibers, σ_1 and σ_2 are the normal stresses of the fibers, which can be expressed as

$$\sigma_1(x,t) = E_f \varepsilon_1 = E_f \frac{\partial u_1(x,t)}{\partial x}, \quad \sigma_2(x,t) = E_f \varepsilon_2 = E_f \frac{\partial u_2(x,t)}{\partial x} \tag{5}$$

where E_f is the Young's modulus of the fibers; ε_1 and ε_2 are the normal strains of fibers. Furthermore, at any point x along fibers length direction, normal stresses acting on the cross section should maintain their mechanical balance with the loading force $P(t)$, leading to the following equation

$$\sigma_1(x,t)\pi r^2 + \sigma_2(x,t)\pi r^2 = P(t) \tag{6}$$

The fiber normal stress σ_1 and σ_2 along the x-direction can be expressed as

$$\sigma_1 = \frac{1}{2} E_f \frac{\partial \delta}{\partial x} + \frac{1}{2}\frac{P}{\pi r^2}, \quad \sigma_2 = -\frac{1}{2} E_f \frac{\partial \delta}{\partial x} + \frac{1}{2}\frac{P}{\pi r^2} \tag{7}$$

The boundary conditions are $\sigma_1(0,t)=0$, $\sigma_1(L,t)=P(t)/\pi r^2$. According to Eq. (7), they can be alternatively written as

$$\frac{\partial \delta(0,t)}{\partial x} = -\frac{P(t)}{E_f \pi r^2}, \quad \frac{\partial \delta(L,t)}{\partial x} = \frac{P(t)}{E_f \pi r^2} \tag{8}$$

While the initial condition can be expressed as follows

$$\delta(x,0) = 0 \tag{9}$$

2.2. Kelvin model

Unlike an elastic material, which instantaneously deforms when a force is applied, biological materials slowly displace until their equilibrium deformation is reached. A Kelvin viscoelastic model containing a spring with shear stiffness G in parallel with a dashpot of viscosity η (Fig. 3c) is applied for interfibrous matrix in an attempt to elucidate the mechanical response of biological composites subjected to transient tensile loading

$$\tau = G\gamma + \eta\dot{\gamma} \tag{10}$$

where G and η are the shear modulus and viscosity coefficient of the interfibrous matrix, respectively. Though many complicated constitutive relations have been developed by considering the component of interfibrous matrix [3, 21, 37-41], Eq. (10) characterizes the basic stress-strain relation underlying Kelvin viscoelastic matrix shear lag model.

Letting

$$\zeta^2 = \frac{\eta}{G}, \quad L_C = \sqrt{\frac{E_f r h}{4G}} \tag{11}$$

and combining Eqs. (1)-(5), we obtain the governing partial differential equation (PDE) for relative sliding δ as follows

$$\frac{\partial \delta}{\partial t} = \frac{L_C^2}{\zeta^2}\frac{\partial^2 \delta}{\partial x^2} - \frac{1}{\zeta^2}\delta \tag{12}$$

where L_C is the characteristic length over which the stresses are transferred between interfibrous matrix and fibers.

A theoretical solution will be employed to solve $\delta(x,t)$, the details of which are given in our previous work [10]. Relative sliding can be derived by solving the nonhomogeneous PDE (Eq. (12)) with nonhomogeneous boundary conditions (Eq. (8)) and initial condition (Eq. (9)).

$$\delta(x,t) = \left[C_0 + D_0(t)\right]e^{-\frac{1}{\zeta^2}t} + \sum_{n=1}^{\infty}\left[C_n + D_n(t)\right]e^{-\left(\frac{1}{\zeta^2}+\frac{L_C^2}{\zeta^2}\frac{n^2\pi^2}{L^2}\right)t}\cos\frac{n\pi x}{L} + \frac{P(t)}{E_f\pi r^2 L}x^2 - \frac{P(t)}{E_f\pi r^2}x \tag{13}$$

where

$$C_0 = \frac{1}{L}\int_0^L\left[-\frac{P(0)}{E_f\pi r^2 L}x^2 + \frac{P(0)}{E_f\pi r^2}x\right]dx \tag{14}$$

$$C_n = \frac{2}{L}\int_0^L\left[-\frac{P(0)}{E_f\pi r^2 L}x^2 + \frac{P(0)}{E_f\pi r^2}x\right]\cos\frac{n\pi x}{L}dx \tag{15}$$

$$D_0(t) = \int_0^t e^{\frac{1}{\zeta^2}s}h_0(s)ds \tag{16}$$

$$D_n(t) = \int_0^t e^{\left(\frac{L_C^2}{\zeta^2}\frac{n^2\pi^2}{L^2}+\frac{1}{\zeta^2}\right)s}h_n(s)ds \tag{17}$$

$$h_0(t) = \frac{1}{L}\int_0^L H(x,t)dx \tag{18}$$

$$h_n(t)=\frac{2}{L}\int_0^L H(x,t)\cos\frac{n\pi x}{L}dx \tag{19}$$

It can be seen from the Eq. (13)-(19) that, C_0 and C_n are determined by the initial condition of force. If no force in the beginning, C_0=C_n=0. D_0 and D_n are resulted from the applied force $P(t)$.

After the solution of relative sliding is obtained, the expressions for normal stress in the fiber and shear stress in the interfibrous matrix can be obtained

$$\sigma_1(x,t)=\sigma_2(x-L,t)=-\frac{n\pi}{2L}\sum_{n=1}^{\infty}\left[C_n+D_n(t)\right]e^{-\left(\frac{1}{\zeta^2}+\frac{L_C^2}{\zeta^2}\frac{n^2\pi^2}{L^2}\right)t}\sin\frac{n\pi x}{L}+\frac{2P(t)}{\pi r^2 L}x-\frac{P(t)}{2\pi r^2} \tag{20}$$

$$\tau(x,t)=-\frac{n^2\pi^2 r}{4L^2}\sum_{n=1}^{\infty}\left[C_n+D_n(t)\right]e^{-\left(\frac{1}{\zeta^2}+\frac{L_C^2}{\zeta^2}\frac{n^2\pi^2}{L^2}\right)t}\cos\frac{n\pi x}{L}+\frac{P(t)}{\pi rL} \tag{21}$$

This implies that the theoretical solution of fibers' displacement u_i (i=1, 2), normal stresses σ_i (i=1, 2) and strains ε_i (i=1, 2), and shear stress τ can be derived if the boundary conditions are known.

2.3. Maxwell model

The Maxwell model consists of a spring and a dash pot in series. We can divide the total strain into two separate strains, one for the spring and one for the dashpot (refer to Fig. 3d). The stress will be the same in both elements. The constitutive relation for Maxwell model is given by

$$\dot{\gamma}=\frac{\dot{\tau}}{G}+\frac{\tau}{\eta} \tag{22}$$

Combining Eqs. (1)-(5), (11) and (22), we obtain the PDE for relative sliding δ

$$\frac{\partial\delta}{\partial t}=L_C^2\frac{\partial^3\delta}{\partial x^2\partial t}+\frac{L_C^2}{\zeta^2}\frac{\partial^2\delta}{\partial x^2} \tag{23}$$

Thus, the governing equation of Maxwell viscoelastic shear lag model is a PDE with mixed derivatives in space and time, which can be solved by numerical Laplace transform method. Boundary and initial conditions are referred as Eqs. (8)-(9).

Let us take the Laplace transform with respect to time of both sides of Eq. (22) due to t>0

$$\Delta_0(x,s)=\mathscr{L}\left[\delta(x,t)\right],\quad P_0(s)=\mathscr{L}\left[P(t)\right] \tag{24}$$

The governing equation can alternatively be written as an ordinary differential equation with parameter s

$$\frac{d^2\Delta_0(x,s)}{dx^2}-\frac{\zeta^2 s}{L_C^2\zeta^2 s+L_C^2}\Delta_0(x,s)=0 \tag{25}$$

and boundary conditions can be transformed into

$$\frac{d\Delta_0(0,s)}{dx}=\frac{-P_0(s)}{E_f\pi r^2},\quad \frac{d\Delta_0(L,s)}{dx}=\frac{P_0(s)}{E_f\pi r^2} \tag{26}$$

According to the theory of ordinary differential equation, we can obtain the analytical solution of Eq. (25) as follows

$$\Delta_0(x,s)=A(s)e^{\frac{\beta_s x}{L_C}}+B(s)e^{-\frac{\beta_s x}{L_C}} \tag{27}$$

where

$$A(s)=\frac{P_0(s)L_C}{E_f\pi r^2}\frac{1}{\beta_s}\frac{1+e^{-\frac{\beta_s L}{L_C}}}{e^{\frac{\beta_s L}{L_C}}-e^{-\frac{\beta_s L}{L_C}}},\quad B(s)=\frac{P_0(s)L_C}{E_f\pi r^2}\frac{1}{\beta_s}\frac{1+e^{\frac{\beta_s L}{L_C}}}{e^{\frac{\beta_s L}{L_C}}-e^{-\frac{\beta_s L}{L_C}}},\quad \beta_s=\sqrt{\frac{\varsigma^2 s}{\varsigma^2 s+1}} \tag{28}$$

Taking Laplace inverse transform on both sides of Eq. (27), we have

$$\delta_0(x,t)=\frac{1}{2\pi i}\int_{a-i\infty}^{a+i\infty}\Delta_0(x,s)e^{st}ds,\ t>0 \tag{29}$$

Now we apply the Fourier series method to numerically calculate Laplace inverse transform. This method is based on choosing the contour of integration in the inversion integral, converting the inversion integral into the Fourier transform, and then approximating the transform by a Fourier series [42]. This method approximates the inversion integral using the following equation:

$$\delta_0(x,t)\approx\frac{2e^{at}}{T}\left[\frac{1}{2}\mathrm{Re}\left[\Delta_0(x,a)\right]+\sum_{k=1}^{\infty}\mathrm{Re}\left[\Delta_0\left(x,a+\frac{k\pi i}{T}\right)\right]\cos\left(\frac{k\pi t}{T}\right)\right] \tag{30}$$

where $i=\sqrt{-1}$. The parameters a and n must be optimized for increasing accuracy. The numerical results are highly accurate for a very short loading time. If the loading time is long, the result of $\delta(x,t)$ might not converge to the accurate result. Nevertheless, finite element result has good convergence for a long loading time, so that we can perform finite element simulations (COMSOL 5.2) to calculate the relative sliding.

Consequently, we calculate the numerical result of $\delta(x,t)$ according to convolution theorem of Laplace transform. According to convolution theorem of Laplace transform, we can get back to the original function of relative sliding

$$\delta(x,t)=\mathscr{L}^{-1}\left[\frac{P_0(s)L_C}{E_f\pi r^2}\Delta_0(x,s)\right]=\int_0^t\frac{P(\tau)L_C}{E_f\pi r^2}\delta_0(x,t-\tau)d\tau \tag{31}$$

2.4. Standard linear solid (SLS) model

According to the theory of viscoelasticity, Kelvin model could not describe the creep behavior of viscoelastic material, while Maxwell model could not capsule the stress relaxation behavior. We are now in a position to look at a more complicated and realistic model, the SLS model. This model consists of a spring in series with a Kelvin unit, which can characterize the creep and stress relaxation behavior of viscoelastic materials. Constitutive equation of SLS model can be given by

$$\tau+\frac{\eta}{G_1+G_2}\dot{\tau}=\frac{G_1G_2}{G_1+G_2}\gamma+\frac{G_1\eta}{G_1+G_2}\dot{\gamma} \tag{32}$$

Combining Eqs. (1)-(5) and (32), we get

$$G_1G_2\delta+G_1\eta\frac{\partial\delta}{\partial t}=\frac{E_f rh(G_1+G_2)}{4}\frac{\partial^2\delta}{\partial x^2}+\frac{\eta E_f rh}{4}\frac{\partial^3\delta}{\partial x^2\partial t} \tag{33}$$

By letting

$$\zeta_1^2=\frac{\eta}{G_1},\quad \zeta_2^2=\frac{\eta}{G_2},\quad L_C=\sqrt{\frac{E_f rh}{4G_1}} \tag{34}$$

Eq. (33) can be simplified as

$$\frac{\partial \delta}{\partial t}=\left(\frac{L_C^2}{\zeta_1^2}+\frac{L_C^2}{\zeta_2^2}\right)\frac{\partial^2 \delta}{\partial x^2}+L_C^2\frac{\partial^3 \delta}{\partial x^2 \partial t}-\frac{1}{\zeta_2^2}\delta \tag{35}$$

In a similar way to solving Maxwell viscoelastic shear lag model, by letting

$$\beta_s=\sqrt{\frac{\zeta_1^2+\zeta_1^2\zeta_2^2 s}{\zeta_1^2+\zeta_2^2+\zeta_1^2\zeta_2^2 s}} \tag{36}$$

the PDE can be transformed to an ordinary differential equation with respect to x

$$\frac{d^2\Delta_0(x,s)}{dx^2}-\frac{\beta_s^2}{L_C^2}\Delta_0(x,s)=0 \tag{37}$$

which is similar to the form of Eq. (25). Thus, the Fourier series method for the Laplace inversion can also be applied to the governing equation (Eq. (37)).

3. Relevant Experiments and Parameters

As a viscoelastic and hierarchical structure, tendon connects muscle to bone and transfers forces to generate smooth motion [43]. Owing to its intermedia stiffness between that of muscle and bone, tendon has a superior mechanical behavior, and serves as a buffer, which is capable of protecting muscle and bone from damage effectively [44].

Histologically, collagen fibril, surrounded by a non-collagen interfibrillar matrix, is the fundamental element for bearing tensile forces in tendon. Both collagen fibrils and the surrounding non-collagen interfibrillar matrix play a crucial role in stress transfer under tensile forces. Gupta et al. [45] stated that, at the fibril level, the interfibrillar matrix governs tendon viscoelastic behavior by generating relative sliding between the adjacent fibrils. On the other hand, stiff fibrils is responsible for carrying a majority of normal stress [22].

According to the relevant experimental observation and measurement by researchers, the geometrical and material parameters of the fibrils and interfibrillar matrix used in this study are listed in Table 2.

Table 2 Parameter values

Parameter	Value	References
E_f	1 GPa	[46]
G	1 Pa	[22]
r	75 nm	[47]
L	50 μm–1.0 mm	[38]
c_f	0.7	[48]
η	0.35 Pa·s	[49]

4. Results and Discussion

4.1. The process of stress transfer

Although numerous experiments have been conducted by using atomic force microscopy (AFM) to measure the micromechanical properties of tendon [50, 51], few researchers explored the effect of loading rate on tendon. When the tendon is subjected to tensile stress, some of its elongation is significantly related to relative sliding between fibrils, which were demonstrated by the earlier studies [52, 53]. In accordance with the constitutive relation of interfibrillar matrix (Eqs. (10), (22) and (32)), shear stress acting on the entire fibril is not only closely relevant to relative sliding, but also significantly affected by relative sliding rate. In order to visualize the variation of shear strength in the joint throughout the overlap length and over time, a constant stress rate $\dot{\sigma}$=5.8333 MPa/s is hence applied to the 1st fibril at one end $x=L$, while the 2nd fibril is fixed at the other end x=0 (see Fig. 3a). The distribution of the relative sliding between fibrils and the normal stress in the 1st fibril at different time is shown in Fig. 4.

As can be seen from Fig. 4, the values of δ and σ_1 are both continuously increasing, while the applied stress is loading at the end $x=L$. The maximum relative sliding occurs at both ends, and the minimum value occurs at the midpoint of the overlap length $x=L/2$ due to the structural symmetry. Of course, the loading process of the tendon is based on the assumptions that the interfibrillar links are permanently engaged in the load transfer mechanism although they can unbind and rebind periodically.

The closer distance to the applied force is, the larger the normal stress of the 1st fibril is. The maximum normal stress of the 1st fibril occurs in the loading end. However, the normal stress in the 2nd fibril is in the opposite condition, which can be found from $\sigma_1(L/2,t)=\sigma_2(L/2,t)$, referring to Eq. (20). For the simplicity of the presentation in figures, the normal stress of the 2nd fibril is not provided therein. Indeed similar mechanical behaviors were reported by other researchers [21-23].

Among these three linear viscoelastic models, the deformation of Maxwell model at the same moment is the largest, in comparison of Kelvin and SLS models, which implies that the Maxwell model has an excellent performance in stress transfer. On the contrary, the relative sliding of Kelvin model is the smallest, the shear stress is concentrated on the both ends of overlap length, and the normal stress of the 1st fibril is concentrated at the loaded end.

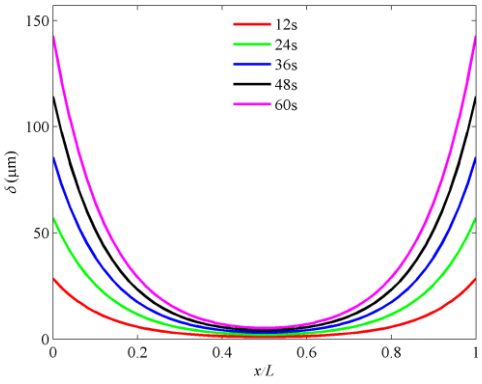

(a) Relative sliding of Kelvin model

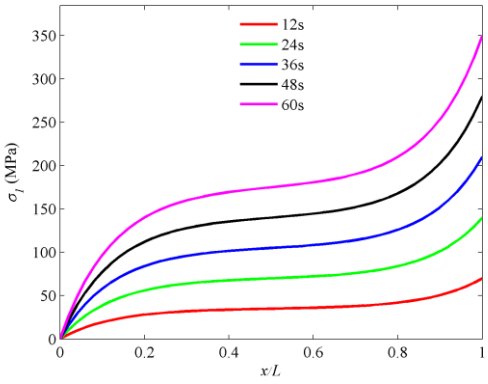

(b) Normal stress in the fibril of Kelvin model

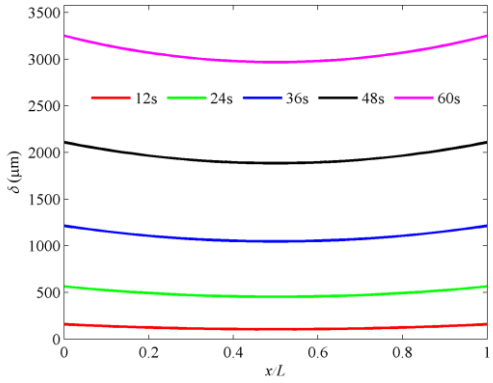

(c) Relative sliding of Maxwell model

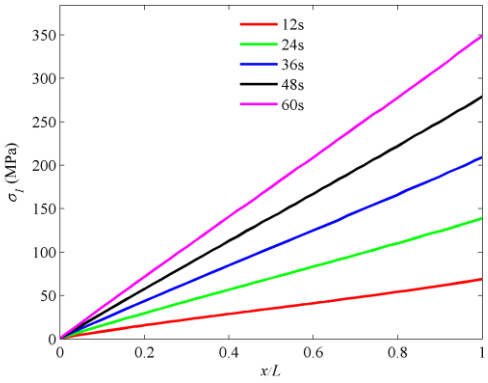

(d) Normal stress in the fibril of Maxwell model

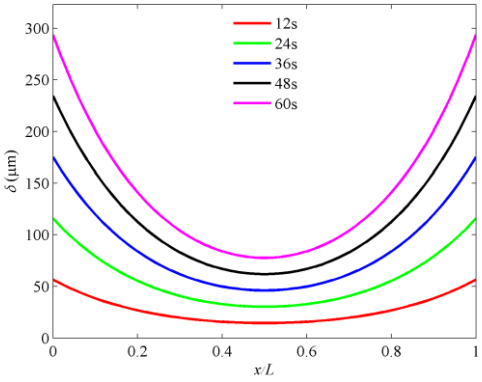

(e) Relative sliding of SLS model

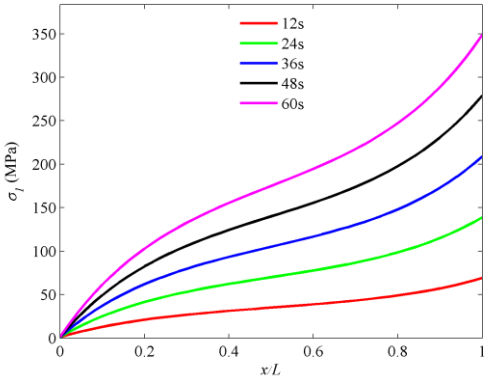

(f) Normal stress in the fibril of SLS model

Fig. 4 Deformation and stress distribution of three kinds of linear viscoelastic shear lag model. (Model parameter used in calculation are L=3.266 mm, $\dot{\sigma}$=5.8333 MPa/s).

4.2. Effect of the fibril overlap length on stress transfer

In our previous study on stress transfer and crack propagation between fiber and matrix, we found that overlap length plays a vital role in the stress transfer [14]. Furthermore, linear elastic mathematical models and finite element models were developed to investigate how fibril overlap length affects the mechanical behavior of tendon [21, 40]. In the present study, the shear lag model taking into account the viscoelasticity is developed to elucidate the overlap length effects on deformation and stress distribution. A unit cell, with different overlap lengths $2L_C$, $8L_C$, $14L_C$ and $20L_C$, is investigated in this section. When the fibril is stretched by a force with a constant stress rate $\dot{\sigma}$=5.8333 MPa/s, the distribution of relative sliding and the 1st fibril normal stress are depicted in Fig. 5.

When the fibril overlap length is short, e.g. L=$2L_C$, the relative sliding δ at the midpoint does not appear to be much different from the values at both ends, and normal stress in the short fibril is linearly distributed along the length direction. In contrast, the relative slidings δ at both ends are much larger than that at the midpoint of overlap length, when the overlap length is long L=$20L_C$, which leads to the 1st fibril normal stress is concentrated at the loaded end severely. Thus, the longer the fibril overlap length is, the smaller the relative sliding is, and the severer the normal stress is concentrated at the loaded end. These conclusions are in excellent agreement with what was reported by Ahmadzadeh et al. [21].

Among these three linear viscoelastic models, the deformation of Maxwell model at the same moment is the largest, followed by the SLS model. The relative sliding of Kelvin model is the smallest, leading to larger normal stress at the loaded end. Thus, the Kelvin model does not seem conducive to stress transfer between the fibril and interfibrillar matrix.

Under static loading conditions, Ji and Gao [54] and Chen et al. [24] investigated the staggered arrangement of biocomposites previously. They proposed that the characteristic length was $L_C = \sqrt{2E_f rh/G}$ in the view of stress transfer. Similarly, Wei et al. [8] predicted $L_C = 2.318\sqrt{E_f rh/G}$ according to an optimization on both strength and toughness fronts. Moreover, under transient rates of loading, characteristic length was predicted based on the maximum shear transfer efficiency point of view, $L_C = \min\left[\tau(x,t)\right]_L$, as was presented by Dutta et al. [36]. In the present study, we introduce viscoelasticity to shear lag model, and use the stress transfer concept to predict characteristic length in the natural fiber biocomposites under transient rates of loading, as given by $L_C = 0.5\sqrt{E_f rh/G}$ for Kelvin and Maxwell models (Eq. (11)) and $L_C = 0.5\sqrt{E_f rh/G_1}$ for SLS model (Eq. (34)). Owing to the influence of viscoelasticity, the characteristic length is shorter than that postulated by Chen et al. [24] and Wei et al. [8].

Characteristic length is a significant parameter for the design strategy of engineering fiber reinforced composites. In contrast to natural biocomposites, high performance fiber reinforced composites typically use continuous fibers, thus achieving high stiffness and strength but presenting limited toughness and ductility. Bio-inspired design of the discontinuous architecture might potentially improve the toughness and ductility, and extend the applicability of fiber reinforced composites to damage tolerant structures [55, 56]. Longer overlap length does not seem conducive to stress transfer. On the other hand, discontinuous fiber would help dissipate energy and protect fibril from overall damage. Also, crack bridging by discontinuous fibers can make brittle materials tougher by transferring stresses from the crack tip to elsewhere in the matrix material.

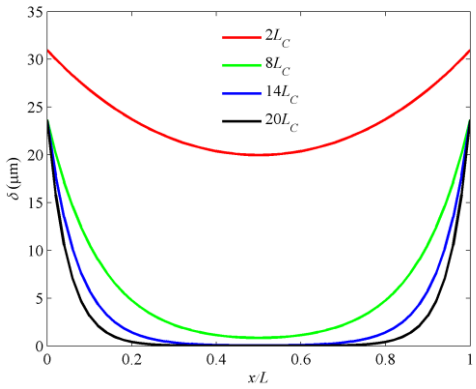

(a) Relative sliding of Kelvin model

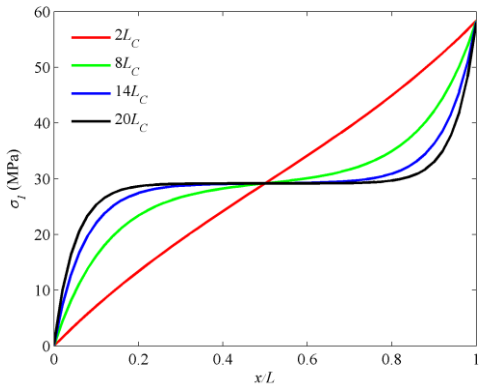

(b) Normal stress in the fibril of Kelvin model

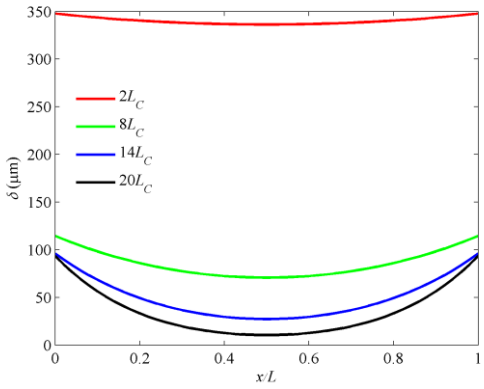

(c) Relative sliding of Maxwell model

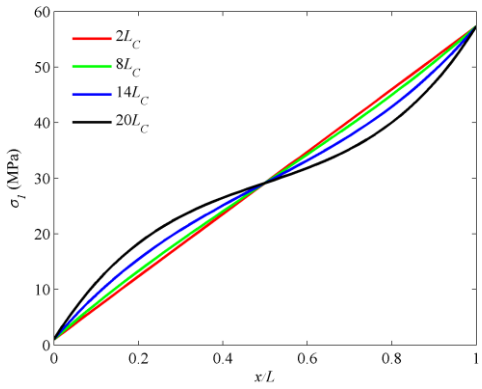

(d) Normal stress in the fibril of Maxwell model

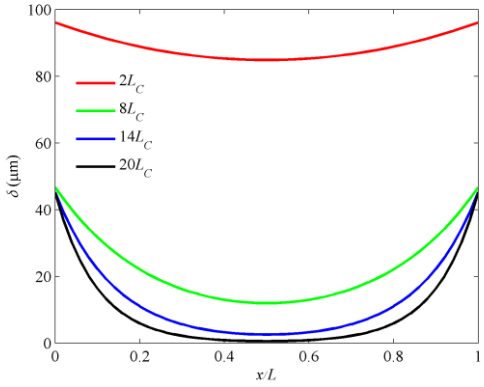

(e) Relative sliding of SLS model

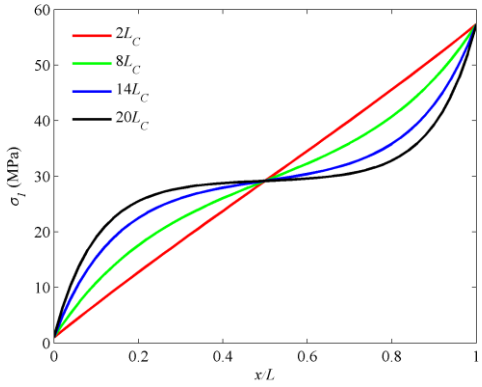

(f) Normal stress in the fibril of SLS model

Fig. 5 Deformation and stress distribution of three kinds of linear viscoelastic shear lag model with different overlap lengths. (Model parameter used in calculation are t=10 s, $\dot{\sigma}$=5.8333 MPa/s, L_C=408.19 μm).

4.3. Effect of the loading rate on stress transfer

In accordance with the governing equations (Eqs. (12), (23) and (35)), the mechanical behavior of tendon is determined by two parameters, L_C^2 and ζ^2 (or ζ_1^2, ζ_2^2), of which the boundary conditions are independent. Notably, the values of these two parameters depend on the geometrical and material parameters of fibril and interfibrillar matrix, excluding the overlap length. Nevertheless, the boundary conditions are only relevant to the tensile force $P(t)$ and the overlap length L. Overall, the mechanical property of tendon relies on the fibril Young's modulus, fibril geometrical dimension and the viscoelasticity of interfibrillar matrix.

In Section 4.1, we have discussed the relative sliding and stress distribution of fibrils and interfibrillar matrix when tendon is stretched by different stresses but at an identical stress rate. We are now to investigate the relative sliding and stress distribution under the same stress but at different stress rates, as illustrated in Fig. 6. Under slow stress rate, e.g. $\dot{\sigma}$=5.8333 MPa/s, the relative sliding δ is large. While tendon is stretched under a fast stress rate, e.g. $\dot{\sigma}$=10000×5.8333, 1000×5.8333 and 100×5.8333 MPa/s, the relative sliding in the region $0.2<x/L<0.8$ is close to zero for Kelvin model. As for Maxwell and SLS

models, the distribution of relative sliding and 1st fibril normal stress appear to be very close, which indicates that, when the loading rate reaches to a certain level, the influence on the structure is very small, even though the loading rate continues to increase. Comparing with these three types of linear viscoelastic model, we can find that Kelvin model is more sensitive to loading rate. When the loading rate is fast enough, Kelvin model might lead to stress concentration at both ends of the overlap length, and do not conductive to stress transfer. It is noteworthy that SLS model (G_1=0.5 Pa and G_2=0.5 Pa) is more conductive to stress transfer at fast loading rate. However, under slow loading rate, Maxwell model is more conductive to stress transfer.

The mechanical properties of tendons with various viscosity coefficients or shear modulus can be obtained according to the analytical and numerical solution to this problem. In order to clarify the relationship between the applied stress rate $\dot{\sigma}$ and viscosity η of interfibrillar matrix, the time and spatial coordinate system is rescaled as $T=\dot{\sigma}t$, $X=x/L$. Variables in the governing equations can be written in a rescaled manner to obtain: $\Delta(X,T)=\delta/L$, $\partial\Delta/\partial T=(\partial\delta/\partial t)/(\dot{\sigma}L)$, $\partial^2\Delta/\partial T^2=L\left(\partial^2\delta/\partial t^2\right)$, and $\partial^3\Delta/\partial X^2\partial T=L\left(\partial^3\delta/\partial x^2\partial t\right)/\dot{\sigma}$. On the basis of the rescale variables, governing equation of Kelvin model can be transformed into dimensionless equation as follows

$$\frac{\dot{\sigma}\eta}{G}\frac{\partial\Delta}{\partial T}=\frac{L_C^2}{L^2}\frac{\partial^2\Delta}{\partial X^2}-\Delta \tag{38}$$

For Maxwell model, the dimensionless form of governing equation is gives as

$$\frac{\dot{\sigma}\eta}{G}\frac{\partial\Delta}{\partial T}=\frac{\dot{\sigma}\eta}{G}\frac{L_C^2}{L^2}\frac{\partial^3\Delta}{\partial X^2\partial T}+\frac{L_C^2}{L^2}\frac{\partial^2\Delta}{\partial X^2} \tag{39}$$

For SLS model, the dimensionless form of governing equation can be expressed as follows,

$$\frac{\dot{\sigma}\eta}{G_2}\frac{\partial\Delta}{\partial T}=\frac{\dot{\sigma}\eta}{G_2}\frac{L_C^2}{L^2}\frac{\partial^3\Delta}{\partial X^2\partial T}+\frac{L_C^2}{L^2}\left(\frac{G_1}{G_2}+1\right)\frac{\partial^2\Delta}{\partial X^2}-\Delta \tag{40}$$

Eqs. (38)-(40) show that the interfibrillar matrix with high viscosity has a similar tendency for relative sliding and fibril normal stress distribution in the tendon when all other parameters remain unchanged.

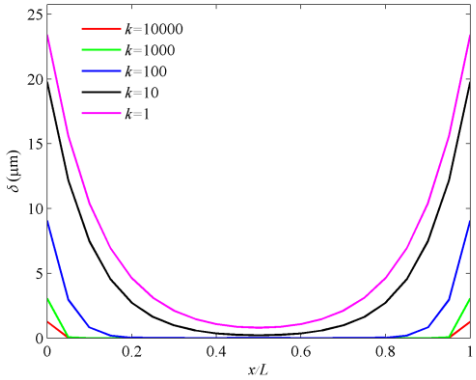

(a) Relative sliding of Kelvin model

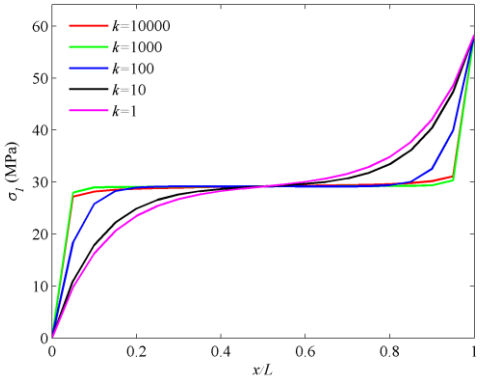

(b) Normal stress in the fibril of Kelvin model

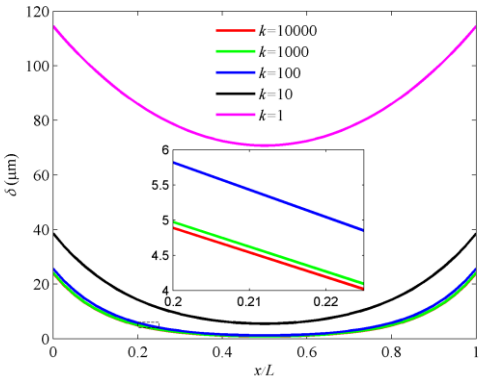

(c) Relative sliding of Maxwell model

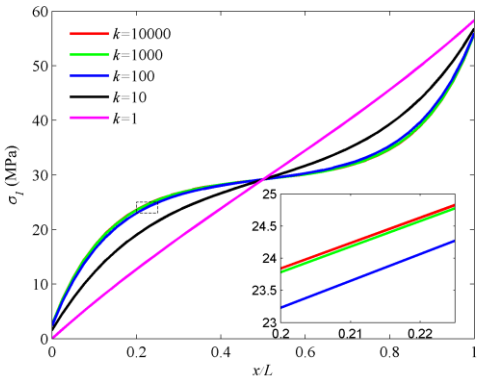

(d) Normal stress in the fibril of Maxwell model

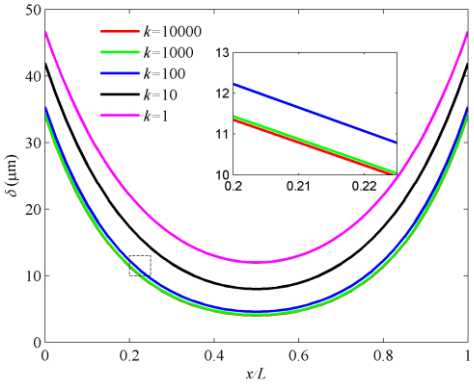

(e) Relative sliding of SLS model

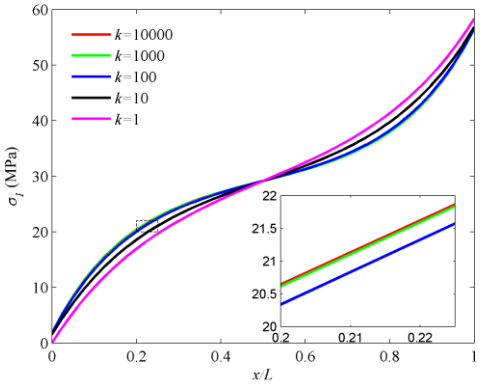

(f) Normal stress in the fibril of SLS model

Fig. 6 Deformation and stress distribution of three kinds of linear viscoelastic shear lag model with different loading rates. (Model parameter used in calculation are L=3.266 mm, t=10/k s, $\dot{\sigma}$=5.8333×k MPa/s, where k is an accommodation coefficient).

4.4. Allocation of shear modulus (G_1 and G_2) of SLS model

When G_1=∞ or G_2=0, the governing equation of SLS model (Eq. (35)) can be written in a simplified manner to obtain the governing equation of Kelvin model (Eq. (12)) and Maxwell model (Eq. (23)), respectively. We investigate the allocation of shear modulus (G_1 and G_2) effects on the relative sling and fibril normal stress distribution herein, as shown in Fig. 7.

It can be noted from Fig. 7 that, relative sliding is the smallest when G_1=0.5 Pa, G_2=0.5 Pa, followed by G_1=0.7 Pa, G_2=0.3 Pa and G_1=0.3 Pa, G_2=0.7 Pa. In addition, the normal stress along the fibril is more inclined to linear distribution when G_1=0.9 Pa, G_2=0.1 Pa and G_1=0.1 Pa, G_2=0.9 Pa.

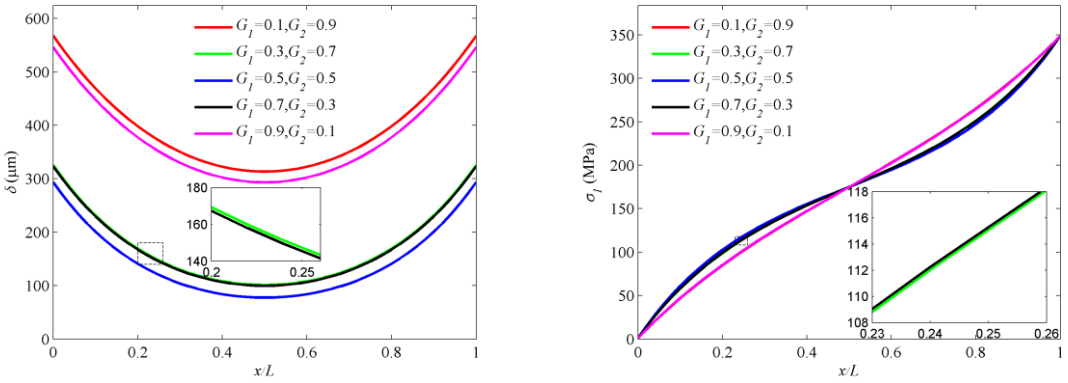

(a) Relative sliding between adjacent fibrils (b) Normal stress in the 1st fibril

Fig. 7 SLS model with different G_1 and G_2. (The unit of shear modules is Pa and model parameter used in calculation are L=3.266 mm, t=60 s, $\dot{\sigma}$=5.8333 MPa/s).

4.5 The effective stiffness

The mechanical behavior of macroscale tissue might be predicted from its micromechanical structure. For instance, the Young's modulus of tendon could be derived from the ratio of the average fibril force over the cross sectional area and the average strain $u_1(L,t)/L$, which can be expressed as

$$E(t)=\frac{c_f L\sigma_1(L,t)}{2u_1(L,t)} \tag{41}$$

where c_f is the fibril volume fraction. Notably, c_f depends on the fibril radius r and the surface-to-surface distance between adjacent fibrils h. Assuming that there are four neighboring fibrils near one fibril, the geometric relationship can be given by

$$\frac{h}{r}=\sqrt{\frac{\pi}{c_f}}-2 \tag{42}$$

It was reported that the geometrical parameters of fibril (lengths and radius) had a critical influence on the elastic modulus of tendon [48, 57]. Also, the Young's modulus of tendon is affected by the geometrical parameters differently under different loading rates, as depicted in Fig. 8. As for Kelvin model, when the tendon is loaded with a slow loading rate, the Young's modulus has a linear growth in the whole loading process (Fig. 8a). However, when the loading rate is fast, the tendon Young's modulus increases nonlinearly owing to the contribution of viscosity of interfibrillar matrix (see Fig. 8b). Fig. 8b depicts that the effective stiffnesses of tendon with overlap lengths $2L_C$, $8L_C$, $14L_C$, $20L_C$ are very close at fast loading rate. Kelvin model could capture the creep behavior but not the stress relaxation effect of soft matter, so its Young's modulus increases very fast. As for Maxwell model, Young's modulus of fibril with overlap length $2L_C$ decreases at applied stress rate 5.8333 MPa/s and 5.8333×1000 MPa/s owing to the stress relaxation effect. Under slow applied stress rate, the Young's modulus of tendon with overlap lengths $8L_C$, $14L_C$, $20L_C$ increases first, and then decreases. However, the Young's modulus of tendon with overlap lengths $8L_C$, $14L_C$, $20L_C$ under fast loading rate continuously increases with a slow growth rate. As for SLS model, no matter how fast or slow of the loading rate, the Young's modulus of tendon with overlap lengths $8L_C$, $14L_C$,

$20L_C$ continuously increases; yet the Young's modulus of tendon with overlap lengths $2L_C$ continuously decreases.

Apart from Kelvin model, Maxwell model and SLS model could describe the process of stress relaxation behavior. Obviously, shorter overlap length is more likely to occur stress relaxation for Maxwell and SLS models (see Fig. 8c-f). Also, we could find that longer overlap length leads to larger effective stiffness of tendon. Furthermore, viscosity property contributes to the effective stiffness of tendon, especially under fast loading rate.

Nacreous layers of some mollusk shells and bone of vertebrates are high-performance structural biological materials. Meyers et al. [58] explored the mechanical design principles for increased stiffness and strength. The Young's modulus of the aragonite bricks is chosen to be 105.39 GPa and the shear modulus of the biopolymer matrix is approximately 1.4 GPa [8]. As for tendon, the Young's modulus of fibril is 1.0 GPa [46] and the shear modulus of interfibrillar matrix is 0.5–1.0 Pa [22]. The shear modulus of bone biopolymer matrix is several orders of magnitude larger than that of tendon interfibrous matrix. Thus, the effective stiffness of tendon is much smaller than that of bone. Hard tissue, e.g. bone, nacre and tooth, can achieve high stiffness and high strength. Nevertheless, soft tissue, e.g. tendon, ligament and muscle, can achieve higher toughness, higher fatigue resistance and longer life.

The microstructure of biological materials is optimized by natural selection to meet their fundamental physiological functions. The shear modulus of hard tissue is comparatively large, the critical overlap length of building blocks in hard tissue, e.g. bone and nacre, is close to the characteristic length L_C [36]. On the other hand, the shear modulus of soft tissue matrix is dramatically small, thus the critical overlap length in the building blocks is several times longer than characteristic length.

Note that the fibril volume fraction c_f contains two cross-sectional geometrical parameters, the fibril radius r and the distance between adjacent fibrils surfaces h (see Eq. (42)). We have previously discussed the effect of fibril volume fraction c_f on effective stiffness [10], and found that no matter how slow or fast of loading rate, tendon effective stiffness with larger fibrils volume fraction will be bigger than that with smaller fibrils volume fraction, and has a similar tendency. As was postulated by Ji and Gao [54] using TSC model, under quasi-static condition, higher volume fraction of ceramic can achieve larger effective stiffness. Due to the length of the article, effect of c_f on the effective stiffness is not discussed herein.

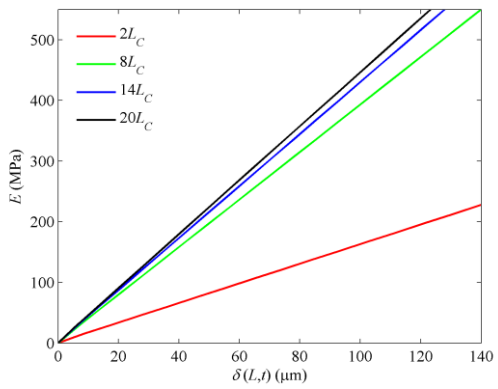

(a) Kelvin model under slow stress rate

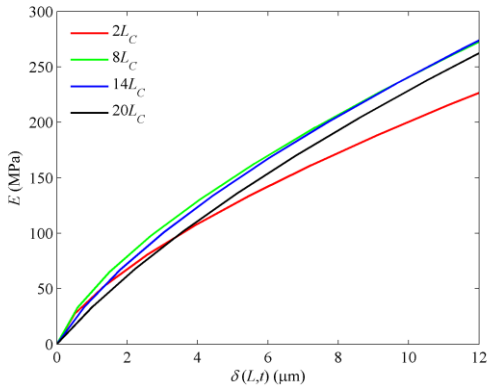

(b) Kelvin model under fast stress rate

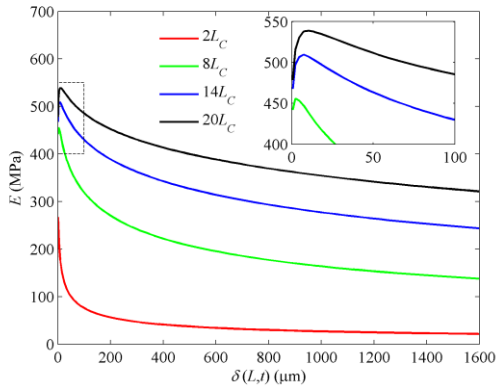

(c) Maxwell model under slow stress rate

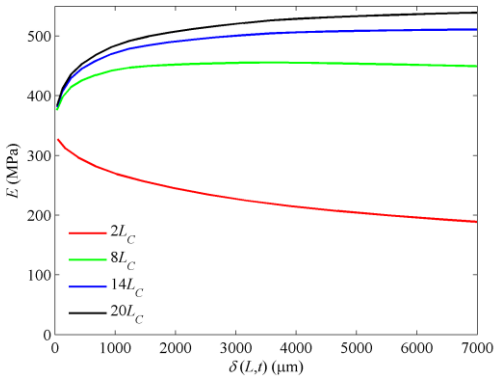

(d) Maxwell model under fast stress rate

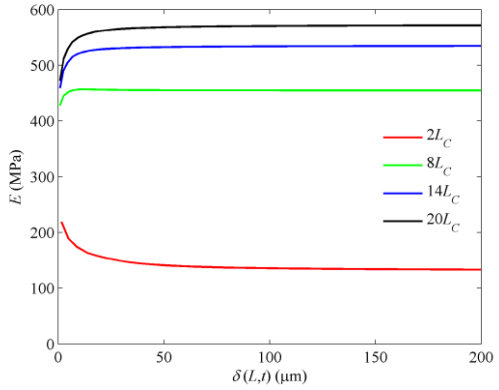

(e) SLS model under slow stress rate

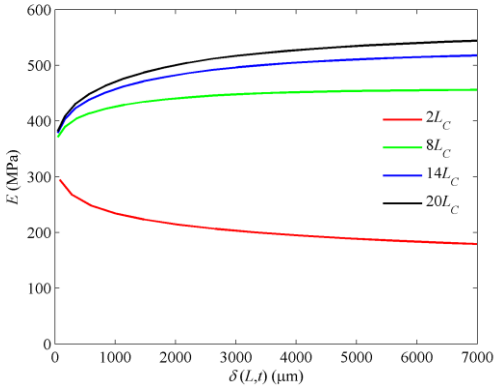

(f) SLS model under fast stress rate

Fig. 8 The effective stiffness of three kinds of linear viscoelastic shear lag model with different overlap lengths (Slow stress rate is $\dot{\sigma}$=5.8333 MPa/s and fast stress rate is $\dot{\sigma}$=5.8333×1000 MPa/s).

4.6. Model validation

A series of *in situ* and *in vitro* uniaxial tensile tests on tendon fascicle were previously conducted to determine the biomechanical behavior of tendon [22, 23, 38, 41, 59]. *In situ* tensile testing and synchrotron X-ray diffraction experiments on rat-tail tendons were implemented by Puxkandl et al. [59] under the applied loading rate in the range 0.0001–0.01 mm/s. Tendon with viscoelastic nature exhibits strain rate-dependent mechanical properties. Hence a microstructural model was established to elucidate the tendon at a fibril level, where fibrils and interfibrillar matrix act as coupled Kelvin viscoelastic system. Although researchers have advanced experiment apparatus, such as AFM, transmission electron microscope (TEM) and microelectromechanical systems (MEMS), etc., it is a tricky experiment for them to measure the shear stress distribution in the interfibrillar matrix and normal stress distribution in the fibrils. Generally, stress-strain relations of tendon fascicle is measured by researchers in the tensile experiments [38, 41, 59].

When the deformation of tendon is small, the Young's modulus of Kelvin model is close to zero, which is not in accord with physical attributes of soft materials. On the other hand, Maxwell model could not reflect the creep behavior of tendon, which is significant to explain the case of the white collar's rotator cuff tears

resulting from using computer for a long time. In our previous work, we have numerically compared Kelvin SLM with experimental results, and pointed out that Kelvin model is reasonable for modelling creep, but does not accurately predict stress relaxation [10]. Thus, SLS model is employed to elucidate the mechanical behavior of tendon. SLS model can explain the phenomena of creep behavior and stress relaxation of biological materials. Hence substitution of the geometrical and material properties of tendon into the governing equation of SLS model, leads to the effective stiffness of tendon and the normal stress of fibril, as seen in Fig. 9. In accordance with the relationship between stress and strain of the native rat tail tendon fascicle measured by Fessel and Snedeker [38], nominal stress-nominal strain curves calculated by the current model is consistent with the experimental results [38]; it also agrees well with the numerical results calculated by Ahmadzadeh et al. [21], as illustrated in Fig. 9a. Moreover, Fig. 9b shows the normal strain distribution in the 2nd fibril, which shows a good agreement with the numerical results obtained from other researchers [40]. Overall, our theoretical predictions show an excellent agreement with relevant experimental and numerical results.

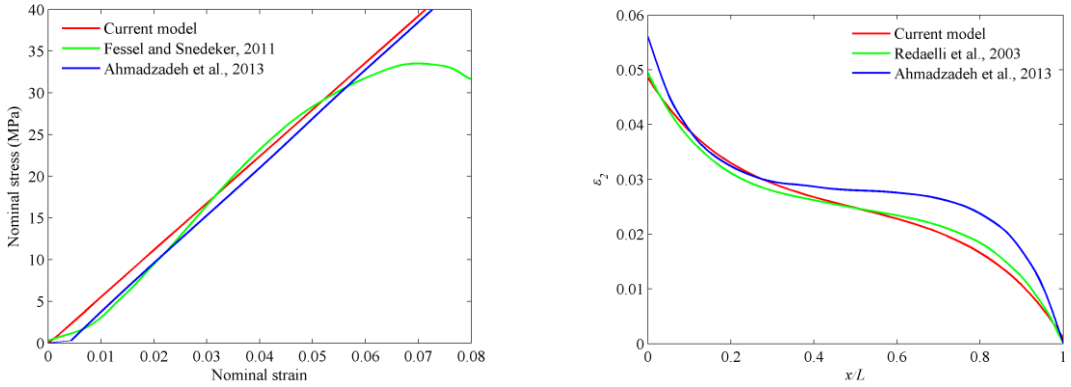

(a) Nominal stress-nominal strain curve (b) Normal stress along the fibril

Fig. 9 Comparison of our current model with experiments [38] and numerical results [21, 40] (Model parameters used in calculation are E_f=1 GPa, L=8400 μm, r=75 nm, c_f=0.5, G_1=G_2=0.5 Pa, η=0.35 Pa·s, $\dot{\sigma}$=5.8333 MPa/s, t=8.5 s).

5. Concluding Remarks

For bone, shell, and teeth, viscosity can generally be neglected during micromechanical analysis. However, viscosity is a non-negligible physical characteristic for soft tissue [60], which might have a crucial effect on the micromechanical properties of biological tissues. Hence, viscoelastic shear lag model needs to be developed to illustrate the micromechanical behavior between fiber and matrix in the biocomposites under transient loading. In this paper, we have extended and improved the previous shear lag model by including viscoelastic behaviors for the interfibrillar matrix and related the effective stiffness of tendon to the velocity of the applied load. This viscoelastic shear lag model is an essential extension to the previous shear lag models which only considered the elastic or elasto-plastic behaviors under static or quasi-static loads. Moreover, we developed an analytical solution to Kelvin shear lag model, and numerical results for

Maxwell and SLS shear lag models. In this way, we address the questions with regards to viscoelastic biocomposites possessing regular staggered alignment microstructure as the most elementary level of architecture under impact loading conditions, by considering a triangular loading pulse: (1) identifying the structure-property correlation for viscoelastic biomaterials under impact loading, (2) the existence of characteristic length of soft matter with viscoelastic property involved in the mechanism of stress transmission between the neighboring reinforcements in transient regime, which could optimize the mechanism of stress transmission between the neighboring reinforcements, and (3) ratify the choice of viscoelastic shear lag model in biocomposites under transient loading. The outcome of the current investigation would provide beneficial guidelines in custom-design manufacture of engineering fiber reinforced composites.

Acknowledgements

The authors gratefully acknowledge the financial support provided by the National Natural Science Foundation of China (No. 11032005), the Major Project of Guizhou Province Department of Science and Technology (2014) 6024 and Academician Workstation of Guizhou Province Department of Science and Technology (2015) 4004. Also, the first author would like to acknowledge the financial support received from China-UK PhD placement programme (Newton Fund PhD programme by British Council and China Scholarship Council) for his study at Plymouth Marine Laboratory.

References

[1] Ritchie RO. The conflicts between strength and toughness. Nature materials. 2011;10:817-22.

[2] Gao H, Ji B, Jäger IL, Arzt E, Fratzl P. Materials become insensitive to flaws at nanoscale: lessons from nature. Proceedings of the National Academy of Sciences. 2003;100:5597-600.

[3] Zhang Z, Liu B, Huang Y, Hwang K, Gao H. Mechanical properties of unidirectional nanocomposites with non-uniformly or randomly staggered platelet distribution. Journal of the Mechanics and Physics of Solids. 2010;58:1646-60.

[4] Wegst UG, Bai H, Saiz E, Tomsia AP, Ritchie RO. Bioinspired structural materials. Nature materials. 2015;14:23-36.

[5] Xu S, Yu JJ. Beneath the Minerals, a Layer of Round Lipid Particles Was Identified to Mediate Collagen Calcification in Compact Bone Formation. Biophysical journal. 2006;91:4221-9.

[6] Veres SP, Lee JM. Designed to fail: a novel mode of collagen fibril disruption and its relevance to tissue toughness. Biophysical journal. 2012;102:2876-84.

[7] Hirokawa N, Shiomura Y, Okabe S. Tau proteins: the molecular structure and mode of binding on microtubules. The Journal of cell biology. 1988;107:1449-59.

[8] Wei X, Naraghi M, Espinosa HD. Optimal Length Scales Emerging from Shear Load Transfer in Natural Materials: Application to Carbon-Based Nanocomposite Design. ACS nano. 2012;6:2333-44.

[9] Yu Z, Liu J, Wei X. Unraveling crack stability and strain localization in staggered composites by

fracture analysis on the shear-lag model. Composites Science and Technology. 2018;156:262-8.
[10] Wu J, Yuan H, Li L, Fan K, Qian S, Li B. Viscoelastic shear lag model to predict the micromechanical behavior of tendon under dynamic tensile loading. Journal of theoretical biology. 2018;437:202-13.
[11] Zuccarello B, Scaffaro R. Experimental analysis and micromechanical models of high performance renewable agave reinforced biocomposites. Composites Part B: Engineering. 2017;119:141-52.
[12] Gao H, Ji B, Buehler MJ, Yao H. Flaw tolerant nanostructures of biological materials. Mechanics of the 21st Century. 2005:131-8.
[13] Cox H. The elasticity and strength of paper and other fibrous materials. British journal of applied physics. 1952;3:72.
[14] Wu J, Yuan H, Liu R. Theory and calculation of stress transfer between fiber and matrix. Applied Mathematics and Mechanics. 2015;36:815-26.
[15] Dutta A, Vanderklok A, Tekalur SA. High strain rate mechanical behavior of seashell-mimetic composites: Analytical model formulation and validation. Mechanics of Materials. 2012;55:102-11.
[16] Ang KK, Ahmed KS. An improved shear-lag model for carbon nanotube reinforced polymer composites. Composites Part B: Engineering. 2013;50:7-14.
[17] Ji S, Zhao P. Location of tensile fracture within rigid-brittle inclusions in a ductile flowing matrix. Tectonophysics. 1993;220:23-31.
[18] Zhao P, Ji S. Refinements of shear-lag model and its applications. Tectonophysics. 1997;279:37-53.
[19] Yuan H, Teng JG, Seracino R, Wu ZS, Yao J. Full-range behavior of FRP-to-concrete bonded joints. Engineering Structures. 2004;26:553-65.
[20] Yuan H, Lu X, Hui D, Feo L. Studies on FRP-concrete interface with hardening and softening bond-slip law. Composite Structures. 2012;94:3781-92.
[21] Ahmadzadeh H, Connizzo BK, Freedman BR, Soslowsky LJ, Shenoy VB. Determining the contribution of glycosaminoglycans to tendon mechanical properties with a modified shear-lag model. Journal of biomechanics. 2013;46:2497-503.
[22] Szczesny SE, Elliott DM. Incorporating plasticity of the interfibrillar matrix in shear lag models is necessary to replicate the multiscale mechanics of tendon fascicles. Journal of the Mechanical Behavior of Biomedical Materials. 2014;40:325-38.
[23] Szczesny SE, Elliott DM. Interfibrillar shear stress is the loading mechanism of collagen fibrils in tendon. Acta Biomaterialia. 2014;10:2582-90.
[24] Chen B, Wu PD, Gao H. A characteristic length for stress transfer in the nanostructure of biological composites. Composites Science and Technology. 2009;69:1160-4.
[25] Schreyer HL, Peffer A. Fiber pullout based on a one-dimensional model of decohesion. Mechanics of Materials. 2000;32:821-36.
[26] Jia Y, Yan W, Liu H-Y. Carbon fibre pullout under the influence of residual thermal stresses in polymer matrix composites. Computational Materials Science. 2012;62:79-86.
[27] Zou Z, Lee H. A cohesive zone model taking account of the effect of through-thickness compression. Composites Part A: Applied Science and Manufacturing. 2017;98:90-8.
[28] Li D, Yang Q-S, Liu X, He X-Q. Experimental and cohesive finite element investigation of interfacial behavior of CNT fiber-reinforced composites. Composites Part A: Applied Science and Manufacturing.

2017;101:318-25.
[29] Sanborn SE, Prévost JH. Discrete modeling of crack bridging by a discontinuous platelet with a controlled interface. International Journal of Solids and Structures. 2008;45:5059-73.
[30] Nian G, Li Q, Xu Q, Qu S. A cohesive zone model incorporating a Coulomb friction law for fiber-reinforced composites. Composites Science and Technology. 2018;157:195-201.
[31] Henry J, Pimenta S. Virtual testing framework for hybrid aligned discontinuous composites. Composites Science and Technology. 2018;159:259-72.
[32] Abid N, Mirkhalaf M, Barthelat F. Discrete-element modeling of nacre-like materials: Effects of random microstructures on strain localization and mechanical performance. Journal of the Mechanics and Physics of Solids. 2018;112:385-402.
[33] Pimenta S, Robinson P. An analytical shear-lag model for composites with 'brick-and-mortar' architecture considering non-linear matrix response and failure. Composites Science and Technology. 2014;104:111-24.
[34] Zhandarov S, Mäder E. Characterization of fiber/matrix interface strength: applicability of different tests, approaches and parameters. Composites Science and Technology. 2005;65:149-60.
[35] Jia Y, Chen Z, Yan W. A numerical study on carbon nanotube–hybridized carbon fibre pullout. Composites Science and Technology. 2014;91:38-44.
[36] Dutta A, Tekalur SA, Miklavcic M. Optimal overlap length in staggered architecture composites under dynamic loading conditions. Journal of the Mechanics and Physics of Solids. 2013;61:145-60.
[37] Ciarletta P, Ben Amar M. A finite dissipative theory of temporary interfibrillar bridges in the extracellular matrix of ligaments and tendons. Journal of the Royal Society Interface. 2009;6:909-24.
[38] Fessel G, Snedeker JG. Equivalent stiffness after glycosaminoglycan depletion in tendon—an ultra-structural finite element model and corresponding experiments. Journal of theoretical biology. 2011;268:77-83.
[39] Goh KL, Meakin JR, Aspden RM, Hukins DW. Stress transfer in collagen fibrils reinforcing connective tissues: effects of collagen fibril slenderness and relative stiffness. Journal of theoretical biology. 2007;245:305-11.
[40] Redaelli A, Vesentini S, Soncini M, Vena P, Mantero S, Montevecchi FM. Possible role of decorin glycosaminoglycans in fibril to fibril force transfer in relative mature tendons—a computational study from molecular to microstructural level. Journal of biomechanics. 2003;36:1555-69.
[41] Shen Zhilei L, Kahn H, Ballarini R, Eppell Steven J. Viscoelastic Properties of Isolated Collagen Fibrils. Biophysical journal. 2011;100:3008-15.
[42] Dubner H, Abate J. Numerical Inversion of Laplace Transforms by Relating Them to the Finite Fourier Cosine Transform. Journal of the ACM. 1968;15:115-23.
[43] Nourissat G, Berenbaum F, Duprez D. Tendon injury: from biology to tendon repair. Nature Reviews Rheumatology. 2015;11:223-33.
[44] Gatt R, Vella Wood M, Gatt A, Zarb F, Formosa C, Azzopardi KM, et al. Negative Poisson's ratios in tendons: An unexpected mechanical response. Acta Biomaterialia. 2015;24:201-8.
[45] Gupta HS, Seto J, Krauss S, Boesecke P, Screen HRC. In situ multi-level analysis of viscoelastic deformation mechanisms in tendon collagen. Journal of structural biology. 2010;169:183-91.

[46] van der Rijt JA, van der Werf KO, Bennink ML, Dijkstra PJ, Feijen J. Micromechanical testing of individual collagen fibrils. Macromolecular bioscience. 2006;6:697-702.
[47] Svensson L, Aszódi A, Reinholt FP, Fässler R, Heinegård D, Oldberg Å. Fibromodulin-null mice have abnormal collagen fibrils, tissue organization, and altered lumican deposition in tendon. Journal of Biological Chemistry. 1999;274:9636-47.
[48] Craig AS, Birtles MJ, Conway JF, Parry DA. An estimate of the mean length of collagen fibrils in rat tail-tendon as a function of age. Connective tissue research. 1989;19:51-62.
[49] Mow VC, Mak AF, Lai WM, Rosenberg LC, Tang LH. Viscoelastic properties of proteoglycan subunits and aggregates in varying solution concentrations. Journal of biomechanics. 1984;17:325-38.
[50] Yang L, van der Werf KO, Dijkstra PJ, Feijen J, Bennink ML. Micromechanical analysis of native and cross-linked collagen type I fibrils supports the existence of microfibrils. Journal of the Mechanical Behavior of Biomedical Materials. 2012;6:148-58.
[51] Yang L, van der Werf KO, Fitié CFC, Bennink ML, Dijkstra PJ, Feijen J. Mechanical Properties of Native and Cross-linked Type I Collagen Fibrils. Biophysical journal. 2008;94:2204-11.
[52] Folkhard W, Mosler E, Geercken W, Knörzer E, Nemetschek-Gansler H, Nemetschek T, et al. Quantitative analysis of the molecular sliding mechanisms in native tendon collagen—time-resolved dynamic studies using synchrotron radiation. International Journal of Biological Macromolecules. 1987;9:169-75.
[53] Mosler E, Folkhard W, Knörzer E, Nemetschek-Gansler H, Nemetschek T, Koch M. Stress-induced molecular rearrangement in tendon collagen. Journal of molecular biology. 1985;182:589-96.
[54] Ji B, Gao H. Mechanical properties of nanostructure of biological materials. Journal of the Mechanics and Physics of Solids. 2004;52:1963-90.
[55] Begley MR, Philips NR, Compton BG, Wilbrink DV, Ritchie RO, Utz M. Micromechanical models to guide the development of synthetic ‘brick and mortar’ composites. Journal of the Mechanics and Physics of Solids. 2012;60:1545-60.
[56] Barthelat F, Dastjerdi AK, Rabiei R. An improved failure criterion for biological and engineered staggered composites. Journal of the Royal Society, Interface. 2013;10:20120849.
[57] McBride DJ, Trelstad RL, Silver FH. Structural and mechanical assessment of developing chick tendon. International Journal of Biological Macromolecules. 1988;10:194-200.
[58] Meyers MA, Chen P-Y, Lin AY-M, Seki Y. Biological materials: Structure and mechanical properties. Progress in Materials Science. 2008;53:1-206.
[59] Puxkandl R, Zizak I, Paris O, Keckes J, Tesch W, Bernstorff S, et al. Viscoelastic properties of collagen: synchrotron radiation investigations and structural model. Philosophical Transactions of the Royal Society of London B: Biological Sciences. 2002;357:191-7.
[60] Babaei B, Velasquez-Mao AJ, Thomopoulos S, Elson EL, Abramowitch SD, Genin GM. Discrete quasi-linear viscoelastic damping analysis of connective tissues, and the biomechanics of stretching. Journal of the Mechanical Behavior of Biomedical Materials. 2017;69:193-202.